ACS APPLIED NANO MATERIALS

www.acsanm.org Article

Coal-Derived Functionalized Nano-Graphene Oxide for Bleach Washable, Durable Antiviral Fabric Coatings

Anthony J. Galante, Kathleen A. Yates, Eric G. Romanowski, Robert M. Q. Shanks, and Paul W. Leu*

Cite This: https://doi.org/10.1021/acsanm.1c03448 Read Online

ACCESS | Metrics & More | Article Recommendations | Supporting Information

Downloaded via UNIV OF PITTSBURGH on January 3, 2022 at 23:08:20 (UTC).
See https://pubs.acs.org/sharingguidelines for options on how to legitimately share published articles.

ABSTRACT: This work demonstrates a coal-derived functionalized nano-graphene oxide coating applied to fabrics that exhibits antiviral properties even after mechanical abrasion or bleach washing. Nano-graphene oxide is chemically exfoliated from low cost coal and functionalized with octadecylamine to render repellency properties. The functionalized nano-graphene oxide is applied to polyethylene terephthalate (PET) fabric after wet etching which roughens the microfiber surface for better coating adhesion and liquid repellency. An additional polydimethylsiloxane (PDMS) layer on top of the functionalized nano-graphene oxide further improves the repellency and durability. The functionalized nano-graphene oxide/PDMS coating robustly repels droplets of water and human saliva. Additionally, we demonstrate antiviral properties with human adenovirus type 5 (HAdV5), herpes simplex virus type 1 (HSV-1), and betacoronavirus (CoV) even after mechanical abrasion and bleach washing. The coating reduces titers of HAdV5 by 1.8 log (98.6%), HSV-1 by 2.2 log (99.4%), and CoV by 2.4 log (99.6%). The coating may have applications in reusable, antiviral personal protective equipment or other large-area, high production coating applications.

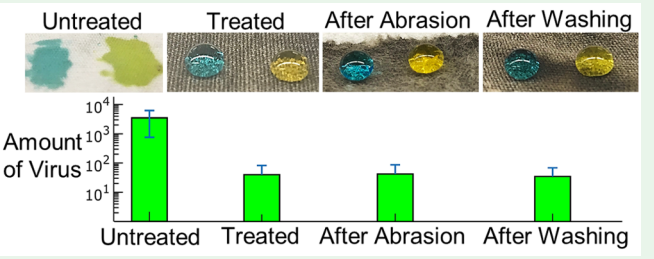

KEYWORDS: *virus, superhydrophobic, repellency, fabric, coal, graphene oxide, coronavirus, antiviral*

INTRODUCTION

Viruses account for an estimated 60% of all human infections.[1] Healthcare professionals are at elevated risk from viral infection due to their work indoors and around infected people.[1] Viruses are a serious threat to humans as they can cause many potentially fatal diseases and cancer.[2,3] Personal protective equipment (PPE) such as gowns, gloves, and masks are essential for protecting healthcare professionals from contacting droplets, aerosols, and viruses that lead to infection. However, PPE may become fomites, which may transfer infection or disease to a host.[4] Virions are expelled into the air from an infected host when breathing, talking, coughing, or sneezing, and virions land on surfaces where they become active sites for spreading infections through hand or skin contamination, ingestion, or mucus membrane contact.

Viruses are particularly difficult to defend against due to their small size and the constant emergence of new viruses.[5] Effective treatments for viruses are significantly more difficult to develop than for bacteria due to their high replication and mutation rates, integration into host DNA, and their abundance.[6] This is evidenced by the lack of antiviral treatments for different viruses that have led to outbreaks such as with SARS-CoV (severe acute respiratory syndrome coronavirus), SARS-CoV 2, MERS-CoV (Middle East respiratory syndrome coronavirus), Chikungunya, Ebola, and Zika.

There is a need to improve public health safety with low-cost, durable textile coatings with biohazard repellency that offer better protection from viruses.[7,8] It is also important that this protection is maintained after washing and mechanical abrasion so they can be reused. Disposable or single-use textiles place a heavy burden on manufacturing supply chains and capacity as can be seen with the recent COVID-19 pandemic. Durable coatings that can undergo laundering and abrasion may help address PPE shortage issues as they can be reused. Reusable textiles also offer significant benefits in terms of less environmental impact and cost savings.[9]

Self-cleaning, medical coatings are a proactive strategy to prevent surface contamination from human body fluid, bacteria, and viruses.[10,11] Recently, two dimensional (2d) carbon nanomaterials, such as graphene and graphene oxide (GO), have been of great interest as these materials have some antimicrobial and antiviral properties from mechanical damage and/or oxidative stress.[12−15] Functionalized carbon nanomaterials have been shown to exhibit antiviral activity against SARS-CoV-2 and human coronavirus HCoV-229E.[14,15]

Received: October 18, 2021
Accepted: December 13, 2021

© XXXX American Chemical Society

https://doi.org/10.1021/acsanm.1c03448
ACS Appl. Nano Mater. XXXX, XXX, XXX−XXX

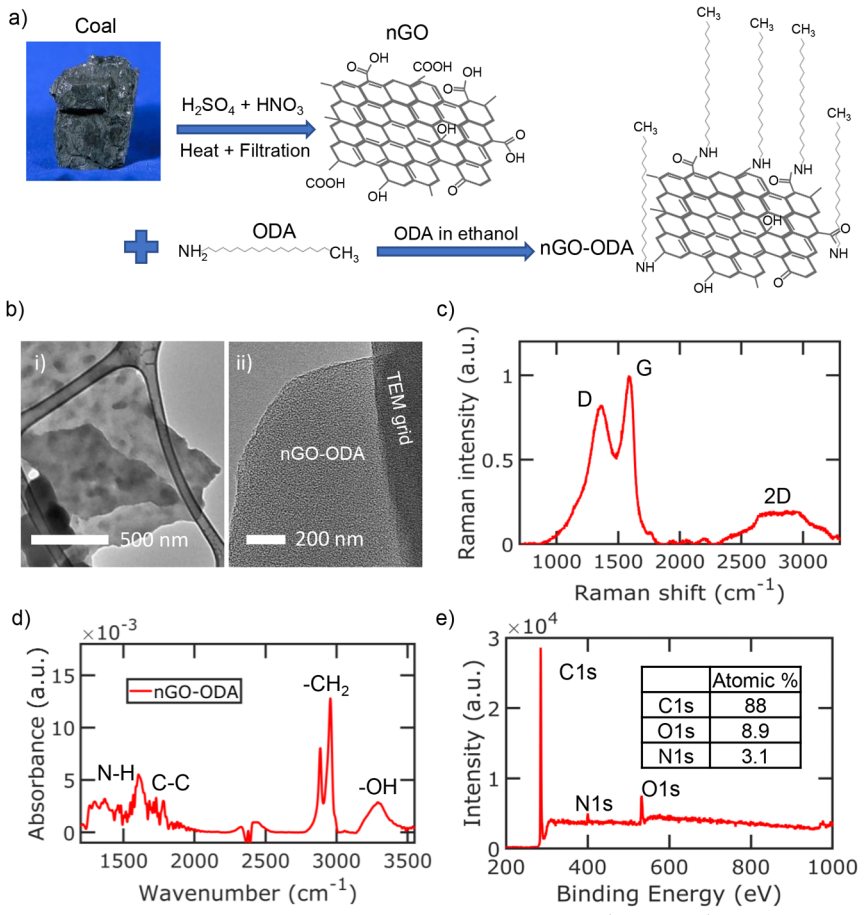

Figure 1. Nano-graphene oxide functionalized with octadecylamine (nGO-ODA) characterization. (a) Schematic of the chemical synthesis of nGO-ODA. (b) Representative TEM images. (c) Raman spectrum of nGO-ODA at Raman shift 500−2500 cm^{-1}. (d) FTIR spectrum of nGO-ODA. (e) XPS spectrum and elemental analysis of nGO-ODA.

However, it remains a challenge to incorporate these 2d carbon nanomaterials onto fabric for PPE applications.

Recent work using 2d carbon nanomaterials for PPE applications have demonstrated the application of graphene to create superhydrophobic, reusable, and recyclable masks[16] and self-reporting bacteria killing masks.[17] Octadecylamine (ODA)-functionalized GO has been dip-coated onto poly-(ethylene terephthalate) (PET) to realize highly hydrophobic fabric.[18] Additionally, fabric has been coated with reduced GO and PDMS (polydimethylsiloxane) to demonstrate super-hydrophobicity with excellent laundering durability up to 250 cycles.[19] However, previous research with graphene derivatives on fabrics have not tested the treatments against infectious virus stocks. Furthermore, all of these works use graphene chemically exfoliated from graphite, which is much more expensive and less realizable for high production applications than graphene chemically exfoliated from coal. Graphite is $1.45 per kg in the US and over 20× more expensive than naturally forming coal, which costs only about $0.06 per kg.[20,21] Coal is a far more abundant feedstock than graphite and produces smaller nano-sized graphene flakes, which may be more useful for antiviral applications.

Repellency properties after bleach washing cycles have also not been tested. Reusable PPE in the healthcare industry are subject to repeated laundering cycles with bleach (sodium hypochlorite)[22] to disinfect and sterilize textiles from bacteria or viruses. However, bleach washing is harsh on fabrics because it delivers high oxidative stress that can damage fabric texture, color, and finish during the sanitization process.[23] Bleach washing may destroy any coatings such that the associated protective functionality is lost. Previous work on functional PPE surface treatments have neglected to analyze the durability of the functionality after washing with bleach.[16,17,24]

In this work, we demonstrate a nano-graphene oxide (nGO) that is coal-derived, as opposed to graphite-derived and is thus cheaper and more realizable for large-scale applications such as fabrics. The nGO is functionalized with long hydrocarbon chains from octadecylamine (ODA) to make octadecylamine-functionalized nano-graphene oxide (nGO-ODA). The ODA functional group adds a liquid-repellent property to the nGO from low surface energy, hydrocarbon chains. nGO-ODA offers the advantage of simultaneous liquid repellency and viral inhibition properties compared to conventional GO or nitrogen doped GO, which only demonstrate virus inhibition.

This work uses dual micro- and nanoscale roughening techniques along with low surface energy coating materials on fabric to render durable superhydrophobicity and antiviral properties for reusable PPE applications. We demonstrate a bleach wash durable, superhydrophobic nGO-ODA coating on PET fabric which actively repels viruses. Three different viruses are tested: human adenovirus type 5 (HAdV5), herpes simplex virus type 1 (HSV-1), and betacoronavirus (CoV). Adenoviruses are nonenveloped icosahedral viruses about 80 nm in size that can cause respiratory and eye infections.[25] Herpes simplex

https://doi.org/10.1021/acsanm.1c03448
ACS Appl. Nano Mater. XXXX, XXX, XXX−XXX

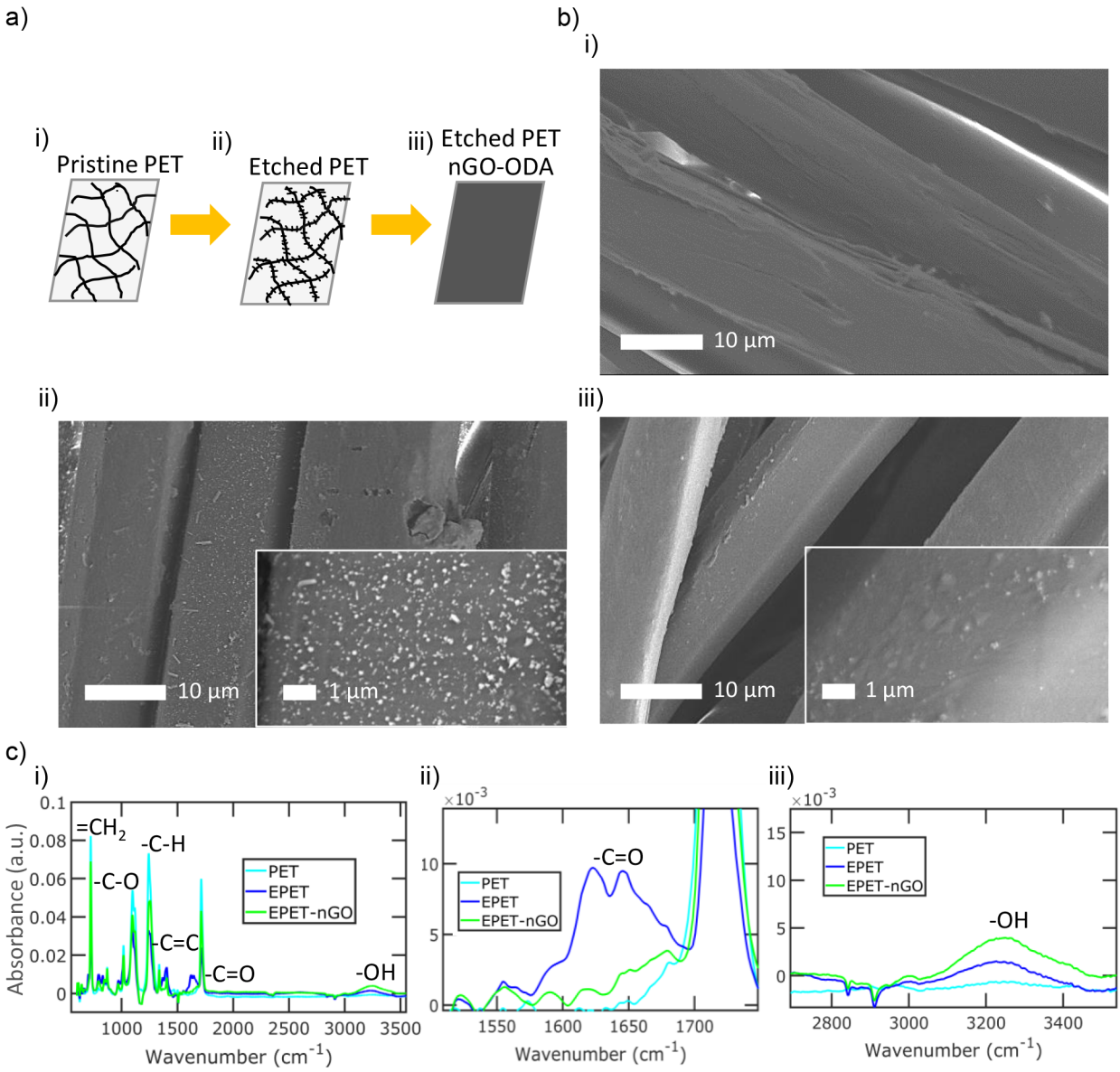

Figure 2. Characterization of PET, EPET, and EPET-nGO samples. (a) Schematic of (i) PET, (ii) etched PET (EPET), and (iii) etched PET nGO-ODA (EPET-nGO) samples. (b) Representative SEM images of (i) PET, (ii) EPET, and (iii) EPET-nGO samples. (c) FTIR spectra of PET samples at wavelengths (i) 600−3600, (ii) 1500−1800, and (iii) 2700−3500 cm^{-1}.

viruses are enveloped viruses about 160 nm in diameter that can cause cold sores and blinding herpetic eye infections.[26] Betacoronaviruses are enveloped viruses and include OC43 and HKU1, which cause the common cold, as well as SARS-CoV, SARS-CoV-2, and MERS-CoV. Coronaviruses are 80−160 nm in size with surface projections protruding from the membrane about 20 nm long.[27]

HAdV5 and HSV-1 are measured by plaque forming units (PFU) to quantify the number of virus particles capable of forming plaques. CoV is measured by the median tissue culture infectious dose ($TCID_{50}$). The coating reduces titers of HAdV5 by 1.8 ± 1.0 log (PFU per mL, 98.6%), HSV-1 by 2.2 ± 0.8 log (PFU per mL, 99.4%), and CoV by 2.4 ± 0.2 log ($TCID_{50}$ per mL, 99.6%). Furthermore, the treated PET fabric maintains antiviral properties after 250 mechanical abrasion or 33 ultrasonic bleach washing cycles. After 250 rotary abrasion cycles, treated samples reduced titers of HAdV5 by 1.7 ± 1.0 log (98.1%), HSV-1 by 1.7 ± 1.0 log (98.0%), and CoV by 2.4 ± 0.2 log (99.6%). Similarly, after 33 bleach washing cycles, treated samples reduced titers of HAdV5 by 1.4 ± 0.2 log (95.7%), HSV-1 by 1.6 ± 0.4 log (97.3%), and CoV by 1.6 ± 0.4 log (97.6%). This work demonstrates a scalable, coal-based nanomaterial fabric coating that shows durable, antiviral properties for reusable, functional PPE.

■ RESULTS AND DISCUSSION

Figure 1 shows results from the characterization of the coal-derived octadecylamine-functionalized nano-graphene oxide (nGO-ODA). Figure 1a illustrates a schematic of the synthesis of octadecylamine-functionalized nano-graphene oxide (nGO-ODA). The nGO flakes are chemically etched from coal feedstocks, resulting in smaller sized flakes (~400 nm) compared to conventional GO (few to ten micrometers) from graphite feedstocks. Figure 1b shows transmission electron microscopy (TEM) images of the multilayer function-

https://doi.org/10.1021/acsanm.1c03448
ACS Appl. Nano Mater. XXXX, XXX, XXX−XXX

a)

Sample	Water Static Contact Angle	Advancing Contact Angle	Receding Contact Angle	Water Hysteresis	Water Breakthrough Pressure
EPET-nGO	156 ± 1°	158 ± 1°	149 ± 2°	9 ± 1°	282 ± 33 Pa

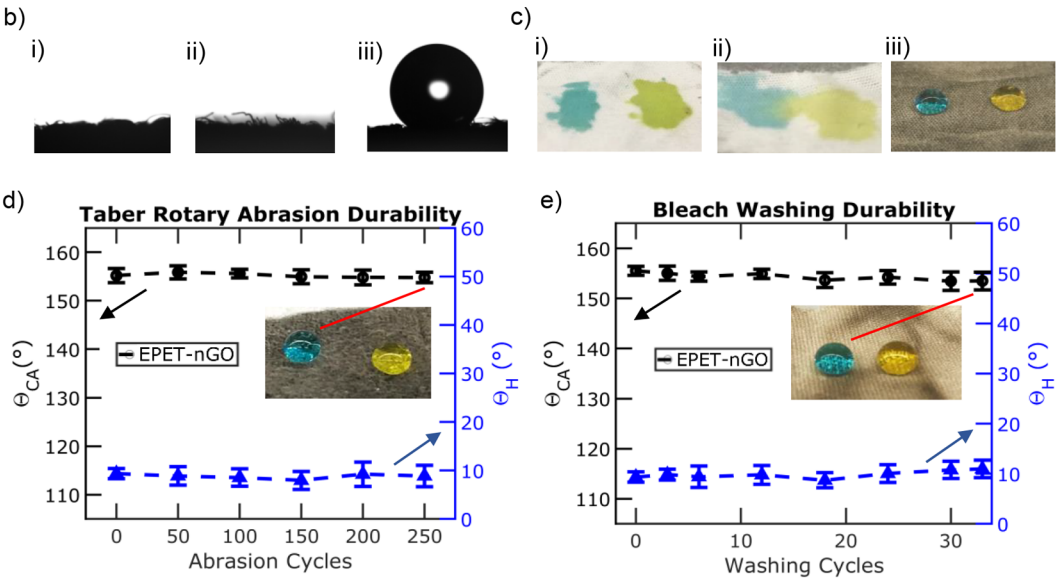

Figure 3. Wetting behavior of EPET-nGO samples compared to untreated PET and EPET. (a) Static and dynamic wetting properties of EPET-nGO. (b) Images of static water contact angles for (i) untreated PET, (ii) EPET, and (iii) EPET-nGO. (c) Optical images of water (blue) and human saliva (yellow) droplets on (i) untreated PET, (ii) EPET, and (iii) EPET-nGO. (d) Water contact angle and hysteresis as a function of Taber rotary abrasion cycles for EPET-nGO samples. (e) Water contact angle and hysteresis as a function of ultrasonic washing cycles in 10% bleach solution for EPET-nGO.

alized nGO-ODA flakes at two different scales. Figures 1bi and 1bii highlight the nanoscale roughness of nGO-ODA. Figure 1c shows the D, G, and 2D bands from Raman characterization of nGO-ODA using a laser wavelength of 532 nm. The crystalline size of nGO-ODA is estimated by the Tuinstra–Koenig relation using the intensity of the D/G band ratio. The crystalline size of the sp^2 region is calculated as 23.7 nm from a D/G band ratio of 0.81.

Figure 1d shows Fourier transform infrared (FTIR) spectroscopy analysis of nGO-ODA. The dominant peaks are $-CH_2$ at wavenumbers 2863 and 2936 cm^{-1} from the ODA. N–H bonds are present from the amine functionalization at wavenumber 1580 cm^{-1}. Carbon–carbon and carbon–oxygen bonds are seen at wavenumbers 1628 and 1724 cm^{-1}, respectively. Stretching hydroxide peaks are confirmed between wavenumbers 3129 and 3457 cm^{-1}. Figure 1e shows elemental analysis of nGO-ODA using X-ray photoelectron spectroscopy (XPS). Prior to functionalization, the nGO sample is about 65.5% carbon and 34.5% oxygen (not shown). After functionalization with ODA, the nGO-ODA sample is mostly made of carbon at 88.0%, followed by oxygen at 8.9% and nitrogen at 3.1% (Figure 1e). The oxygen content is lost during functionalization due to the reaction to form amide bonds between the carboxylic groups of the nGO and the amine groups of the ODA.

In this study, we use polyethylene terephthalate (PET) as fabric material since it is commonly used for medical and healthcare applications such as gowns, scrubs, and caps.[28] Figure 2 shows the surface characterization results of PET, etched PET (EPET), and etched PET nGO-ODA (EPET-nGO) fabric samples. A schematic of the different samples is shown in Figure 2a. Sample fabrication begins by cleaning the PET fabric with isopropyl alcohol, methanol, and acetone. Then, PET is chemically etched with KOH and KMn_4O_5 to roughen the surface. Roughening the microfibers prior to coating renders the surface superhydrophobic once the nGO-ODA coating is added. Microfibers from pristine PET (Figure 2a-i) samples are etched to created etched PET (EPET) with additional roughness on the microfibers at the micrometer scale (Figure 2a-ii). Then, etched samples are dip-coated in nGO-ODA, followed by oven curing to make etched PET nGO-ODA (EPET-nGO) samples. The addition of nGO-ODA material lowers the overall surface energy and adds roughness at the nanoscale, important for repelling small scale (<600 nm) particulates.[29] Fabrics are dyed black in color from the nGO-ODA coating (Figure 2a-iii). A more detailed schematic of the sample fabrication is provided in Figure S2.

Figure 2b shows the surface morphology of fabric samples using scanning electron microscopy (SEM). The untreated PET woven fabric consists of fibers about 12–15 μm in diameter (Figure 2bi). After etching PET with KOH and KMn_4O_5, the fabric microfibers are roughened (Figure 2b-ii). The roughened PET microfibers after coating with nGO-ODA and curing are shown in Figure 2b-iii (EPET-nGO samples).

The surface chemistry of fabric samples is characterized by FTIR spectroscopy (Figure 2c). The entire FTIR spectra of PET samples are shown in Figure 2c-i. Pristine PET samples have a distinct peak at wavenumber 712 cm^{-1} from ester

https://doi.org/10.1021/acsanm.1c03448
ACS Appl. Nano Mater. XXXX, XXX, XXX–XXX

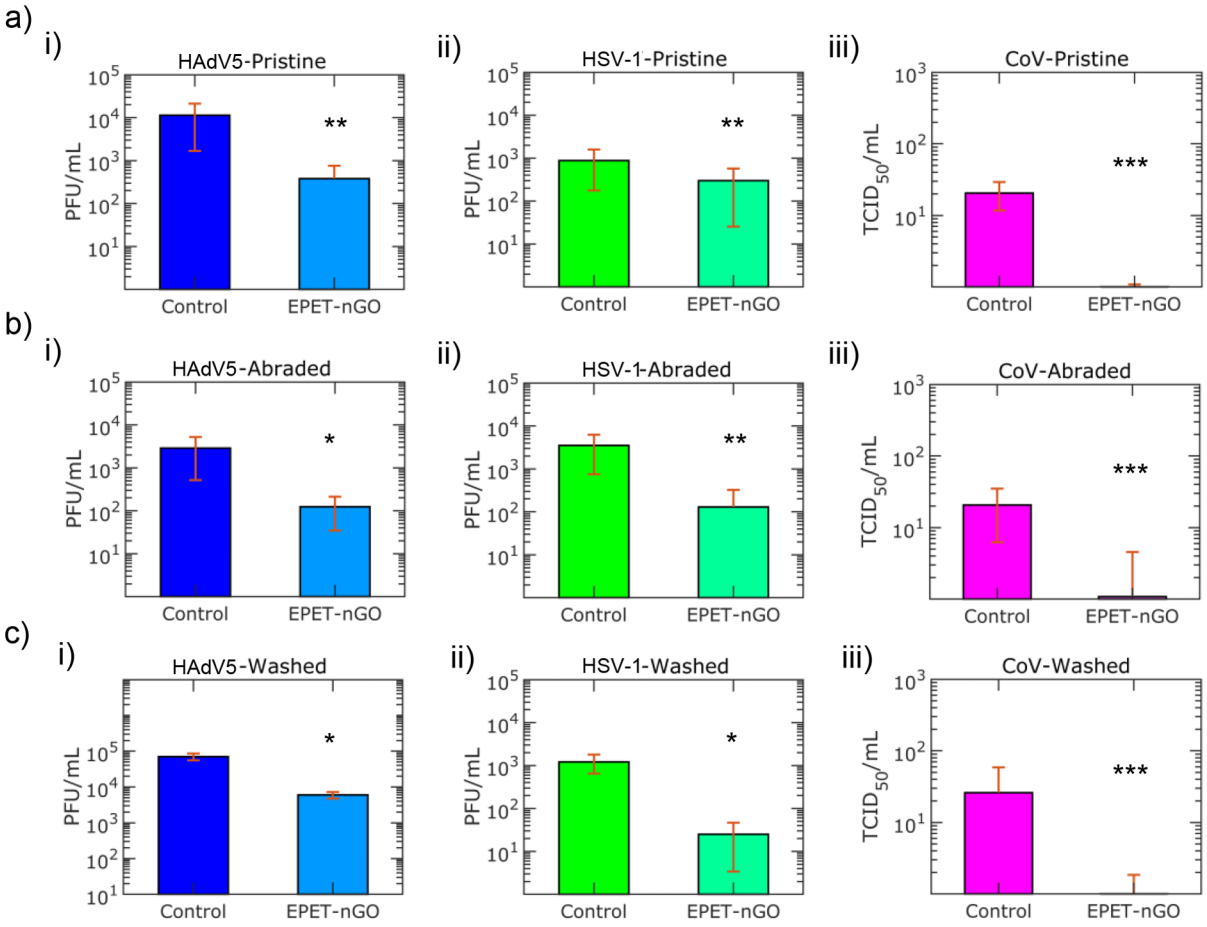

Figure 4. Antiviral property of EPET-nGO-treated samples compared to untreated controls. (a) Mean virus quantities and standard deviation for HAdV5 (i), HSV-1 (ii), in plaque forming units per mL (PFU/mL), and CoV (iii), in $TCID_{50}$ per mL ($TCID_{50}$ /mL). (b) Mean virus quantities and standard deviation on control PET and EPET-nGO samples for HAdV5 (i), HSV-1 (ii), and CoV (iii) after 250 rotary mechanical abrasion cycles (abraded). (c) Mean virus quantities and standard deviation on control PET and EPET-nGO samples for HAdV5 (i), HSV-1 (ii), and CoV (iii) after 33 bleach washing cycles (washed). Asterisks indicate the statistical significance that the control is the same as EPET-nGO treatments from Mann−Whitney statistical tests, one asterisk for $p \leq 0.05$, two for $p < 0.01$, and three for $p < 0.001$.

groups. The methylene group and C−O bond are observed at wavenumbers 1030 and 1090 cm^{-1}. The terephthalate group is confirmed at wavenumber 1240 cm^{-1}. Vibrations from carbon double bonds are seen at 1504 cm^{-1} and stretching of C═O groups at 1730 cm^{-1}. EPET samples introduce stretching C═C and C═O groups at wavenumbers 1640 and 1661 cm^{-1}, respectively (Figure 2c-ii). EPET-nGO samples show the presence of nGO-ODA at 3129−3457 cm^{-1} (Figure 2c-iii). The amine group vibration from the GO-ODA cannot be identified due to the dominant signal from the hydrocarbon groups of the polyester substrate.

The wetting behavior of PPE is important for repelling fluids that may contribute to the transmission of infection. Figure 3 shows the wetting properties of EPET-nGO fabric samples. Figure 3a lists the average water static contact angle, advancing contact angle, receding contact angle, hysteresis, and breakthrough pressure for respective samples. The static contact angle is the angle of a liquid droplet on a surface when the contact area between the liquid and surface is unmoved. The advancing angle describes the angle when a droplet is wetting the surface, and the receding angle is the angle when a droplet is dewetting the surface. The hysteresis describes how easily a droplet rolls off the surface and is calculated by the difference between the advancing and receding contact angles.

Untreated PET and etched PET samples are fully wetting with water droplets; faster liquid spreading is observed for etched PET fibers. After treatment, the EPET-nGO samples are superhydrophobic, with an average water static contact angle of 156 ± 1° and water hysteresis of 9 ± 1°. The combination of roughened microfibers and nGO-ODA nanomaterial creates a low surface energy surface with dual micro- and nanoscale roughness, important for rendering a robust, superhydrophobic wetting property.[30,31] The Wenzel wetting state is when the liquid is fully wetting and in complete contact with the roughness of a surface. After etching and coating with nGO-ODA, a low-energy surface with both micro- and nanoscale roughness is created that promotes Cassie−Baxter wetting instead of Wenzel wetting. The Cassie−Baxter wetting state is when liquid sits on top of the roughness of a surface, resulting in air pockets between the surface and the liquid. The low fraction of contact area between the surface and liquid results in high static contact angle and low contact angle hysteresis which is characteristic of superhydrophobic behavior, where droplets ball up on the surface and easily roll off.

The amount of Laplace pressure required for liquid to infiltrate the air pockets and transition from Cassie−Baxter to Wenzel wetting state is called the breakthrough pressure. The

https://doi.org/10.1021/acsanm.1c03448
ACS Appl. Nano Mater. XXXX, XXX, XXX−XXX

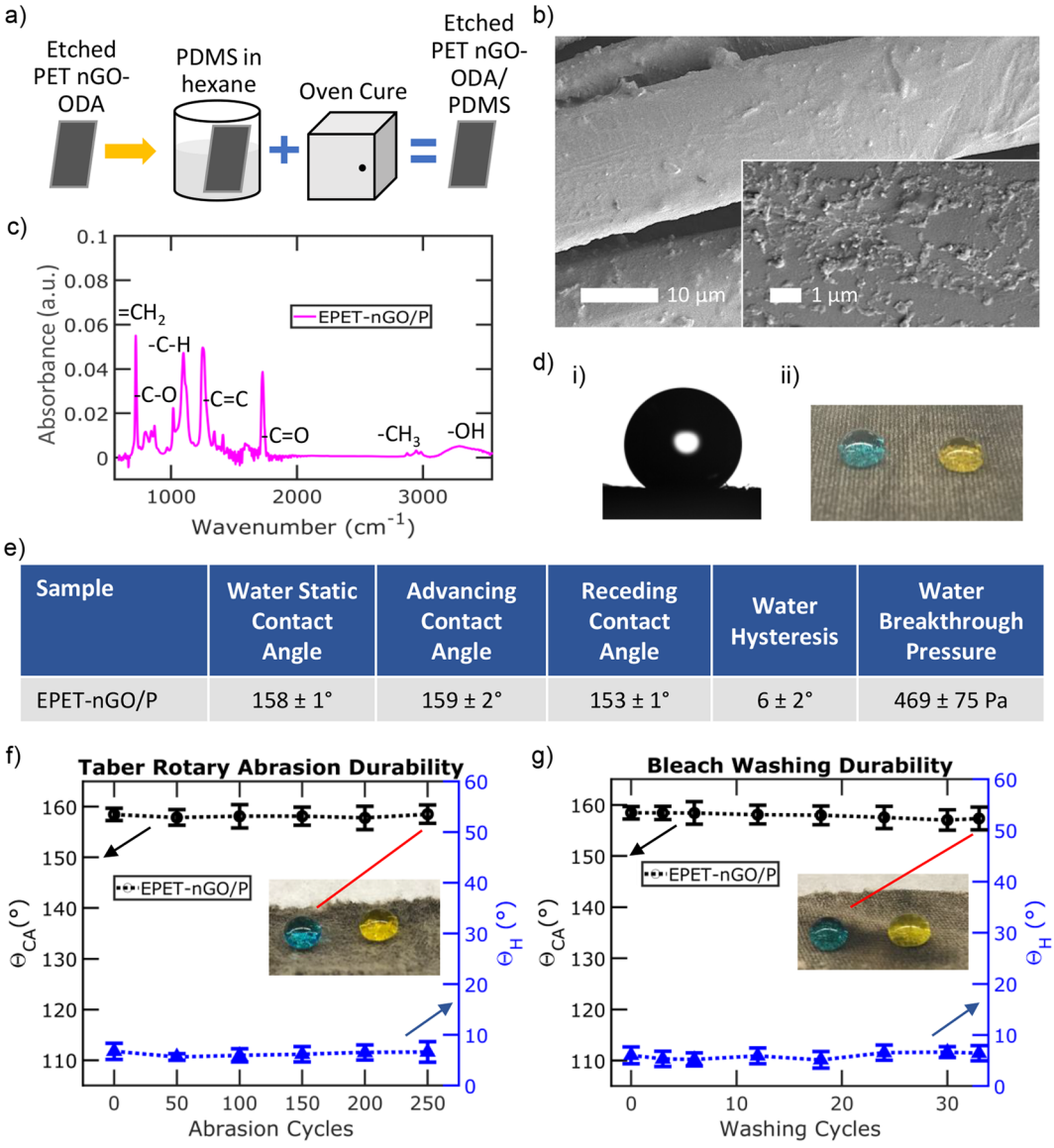

Sample	Water Static Contact Angle	Advancing Contact Angle	Receding Contact Angle	Water Hysteresis	Water Breakthrough Pressure
EPET-nGO/P	158 ± 1°	159 ± 2°	153 ± 1°	6 ± 2°	469 ± 75 Pa

Figure 5. Characterization and wetting behavior of EPET-nGO/P samples. (a) Fabrication schematic for etched PET nGO-ODA PDMS (EPET-nGO/P) samples. (b) Representative SEM image of EPET-nGO/P samples. (c) FTIR spectrum of EPET-nGO/P. (d) (i) Goniometer image of a water droplet on EPET-nGO/P and (ii) image of single water (blue) and human saliva (yellow) droplets on EPET-nGO/P. (e) Table of wetting properties of EPET-nGO/P samples. (f) Water contact angle and hysteresis as a function of Taber rotary abrasion cycles for EPET-nGO/P samples. (g) Water contact angle and hysteresis as a function of ultrasonic washing cycles in 10% bleach solution for EPET-nGO/P.

breakthrough pressure is a measure of the stability of the Cassie−Baxter wetting state.

Breakthrough pressure characterization shows that the EPET-nGO samples transition from Cassie−Baxter to Wenzel wetting state at an estimated droplet radius at breakthrough of 510 μm for an overall breakthrough pressure of 282 ± 33 Pa. Representative images from breakthrough pressure experiments are provided in Figure S3. Figure 3b shows goniometer images of single 5 μL water droplets on (i) untreated PET, (ii) EPET, and (iii) EPET-nGO samples. Figure 3c shows representative optical images of dyed water (blue) and human saliva (yellow) droplets on (i) PET, (ii) EPET, and (iii) EPET-nGO samples.

In addition to superhydrophobicity after fabrication, EPET-nGO samples maintain this superhydrophobicity after both mechanical abrasion and ultrasonic bleach washing. Taber rotary abrasion is a standard method for analyzing the durability of fabric coatings under mechanical wear, and bleach washing is a standard protocol for reusable, personal protective equipment in healthcare settings. The durability of the repellency properties for EPET-nGO samples after mechanical rotary abrasion and ultrasonic bleach washing is summarized in Figure 3d,e.

Figure 3d consists of the water static contact angle and hysteresis of EPET-nGO samples as a function of Taber rotary abrasion cycles from a ceramic wheel (CS-10) under a load of 500 g. The average changes in static water contact angle and hysteresis of EPET-nGO are 2 ± 1° and 3 ± 1°, respectively, after 250 abrasion cycles. Representative optical images of water (blue) and human saliva (yellow) droplets on EPET-nGO after 250 abrasion cycles are also shown (Figure 3d). After 250 rotary abrasion cycles the PET fabric begins to tear and form holes. Additional SEM images of samples after 250 abrasion cycles are provided in Figure S4.

https://doi.org/10.1021/acsanm.1c03448
ACS Appl. Nano Mater. XXXX, XXX, XXX−XXX

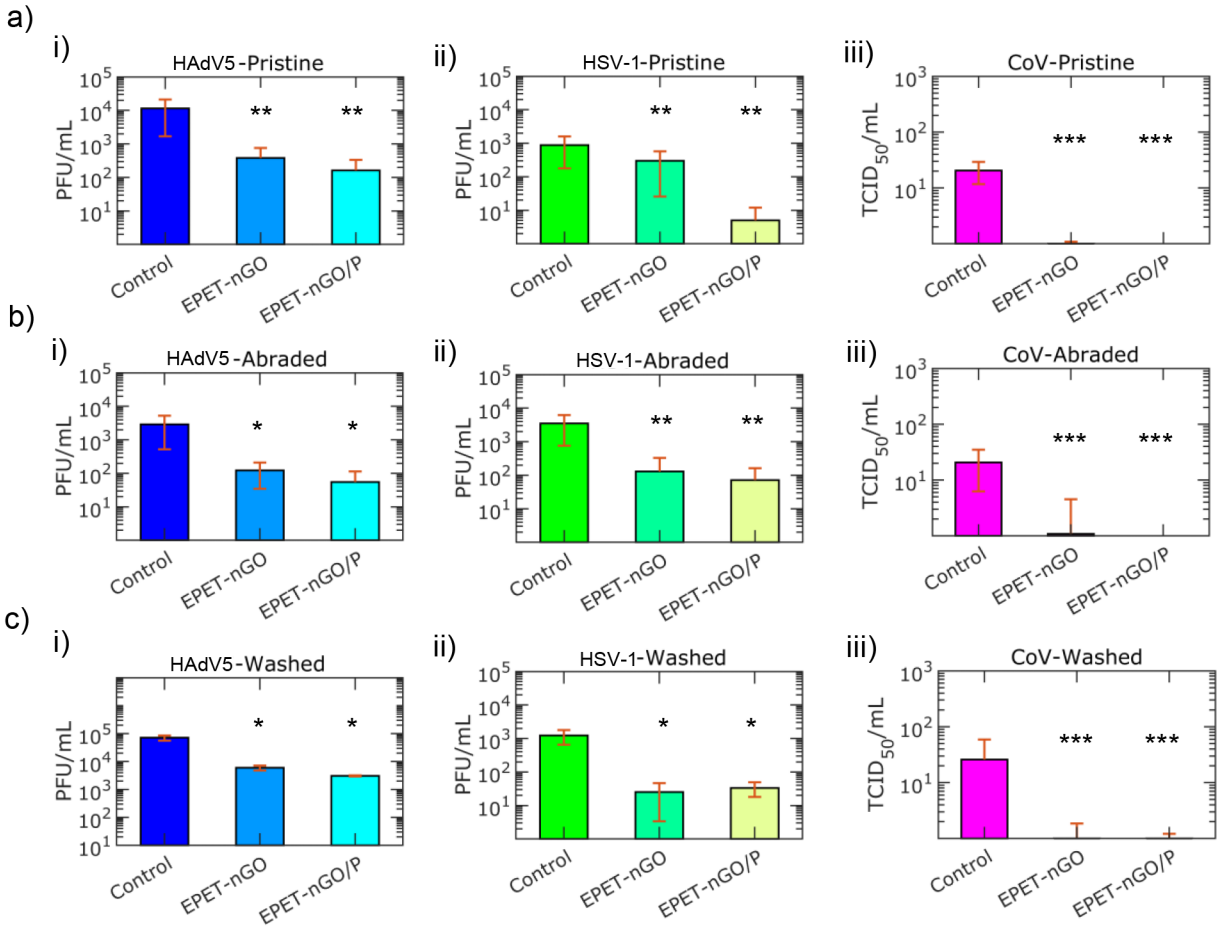

Figure 6. Antiviral property of EPET-nGO and EPET-nGO/P-treated samples compared to untreated controls. (a) Mean and standard deviation virus quantities from control PET, EPET-nGO, and EPET-nGO/P samples samples for HAdV5 (i), HSV-1 (ii), in plaque forming units per mL (PFU/mL), and CoV (iii), in $TCID_{50}$ per mL ($TCID_{50}$ /mL). (b) Mean and standard deviation virus quantities from control PET, EPET-nGO, and EPET-nGO/P samples for HAdV5 (i), HSV-1 (ii), and CoV (iii) after 250 rotary mechanical abrasion cycles (abraded). (c) Mean and standard deviation virus quantities from control PET, EPET-nGO, and EPET-nGO/P samples for HAdV5 (i), HSV-1 (ii), and CoV (iii) after 33 bleach washing cycles (washed). Asterisks indicate the statistical significance that the control is the same as either EPET-nGO or EPET-nGO/P treatments from Mann−Whitney statistical tests, one asterisk for $p \leq 0.05$, two for $p < 0.01$, and three for $p < 0.001$.

Figure 3e consists of the water static contact angle and hysteresis of EPET-nGO samples as a function of ultrasonic bleach washing cycles. The average changes in static water contact angle and hysteresis are 2 ± 1° and 2 ± 1°, respectively, after 33 bleach washing cycles. Etching prior to dip-coating and thermally curing after coating improve the wetting stability of nGO-ODA on PET. Water (blue) and human saliva (yellow) droplets on EPET-nGO samples after 33 bleach washing cycles continue to have high static contact angles (Figure 3e). Color fastness, indicating a loss of nGO-ODA, after bleach washing cycles is observed for EPET-nGO samples; however, the liquid repellency properties are still maintained with water and human saliva. Also, the presence of nGO-ODA can still be observed on EPET-nGO after 33 bleach washing cycles, shown by FTIR in Figure S5. Bleach washing removes some nGO-ODA from PET; however, there is still sufficient nGO-ODA absorbed on the fibers after 33 bleach washes to maintain a Cassie−Baxter wetting state to repel liquids.

Virus assays are conducted by submerging the samples with virus particles diluted in phosphate buffered saline (PBS) while rocking for 1 h, and then the samples are dunked twice in fresh PBS to remove nonattached particles. Lastly, samples are sonicated at low power to remove viruses that are adherent to the samples. The leftover liquid is used to quantify the amount of virus present on the fabric samples. Mann−Whitney statistical tests are used to assess whether the fabric treatment reduces the amount of virus particles on the fabric compared to controls. Asterisks indicate the level of statistical significance with which the treatment group is the same as the control group with one asterisk for $p \leq 0.05$, two for $p < 0.01$, and three for $p < 0.001$. We test three types of virus stocks: HAdV5 (nonenveloped), HSV-1 (enveloped), and CoV (enveloped). HAdV5 and HSV-1 are characterized by using standard plaque forming units (PFU) assays, while CoV is characterized by using median tissue culture infectious dose ($TCID_{50}$) assays. Treated fabrics are tested before (pristine) and after 250 rotary abrasion cycles (abraded) or 33 bleach washing cycles (washed).

Figure 4a shows the antiviral property of pristine EPET-nGO samples compared to PET controls with (i) HAdV5, (ii) HSV-1, and (iii) CoV. For EPET-nGO samples, the antiviral properties consist of reducing HAdV5 by 1.5 log ± 1.0 (97.0%), HSV-1 by 0.5 ± 0.3 log (66.1%), and CoV by 1.6 ± 0.6 log (97.6%) compared to controls, as shown in Figure 4a-i-iii. Figure 4b shows the antiviral properties of rotary abraded

https://doi.org/10.1021/acsanm.1c03448
ACS Appl. Nano Mater. XXXX, XXX, XXX−XXX

samples for HAdV5 (i) HSV-1 (ii) and Cov (iii). EPET-nGO samples reduce titers of HAdV5 by 1.4 ± 0.8 $\log_{10}$ (95.7%), HSV-1 by 1.4 ± 0.9 $\log_{10}$ (96.3%), and CoV by 1.3 ± 0.6 log (94.8%) after 250 rotary abrasion cycles, as shown in Figure 4b-i−iii. Figure 4c shows the antiviral properties of bleach washed samples for HAdV5 (i) HSV-1 (ii) and Cov (iii). EPET-nGO samples reduce titers of HAdV5 by 1.1 ± 0.2 log (91.6%), HSV-1 by 1.7 ± 0.6 log (98.0%), and CoV by 1.5 ± 0.7 log (96.5%) after 33 bleach washing cycles, as shown in Figure 4c-i−iii. The PET-nGO samples can demonstrate antiviral behavior for a range of virus stocks, even after harsh durability tests. Also, the nGO-ODA material remains on the fabric after durability testing to maintain virus inhibition behavior.

Because some of the nGO-ODA material on EPET-nGO samples can be removed from the fabric when subject to extended washing cycles with bleach, a thin layer of PDMS is applied to the fabric to improve the bleach wash durability by additional chemical resistance. The PDMS layer provides chemical resistance and durability so the treatment may be reusable in bleach washing procedures. The PDMS is added by dip-coating and thermal curing to make etched PET nGO-ODA PDMS (EPET-nGO/P) samples for enhanced repellency and durability. A schematic of the additional treatment step is shown in Figure 5a. EPET-nGO samples are dipped in a 1:10 ratio of PDMS (Sylgard) diluted in hexane and cured in an oven for 2 h to make EPET-nGO/P samples.

Figure 5b shows the surface morphology of fabric microfibers after etching, dip-coating with nGO-ODA, curing, dip-coating in PDMS, and subsequent curing for EPET-nGO/P samples. Figure 5c shows the surface chemistry of EPET-nGO/P samples by FTIR. Additional methyl groups from the PDMS treatment are observed at wavenumber 2850 cm^{-1}. Methyl groups lower the surface energy of the fabric which further improves the liquid repellency property. Figure 5d shows goniometer images of water (i) and droplets of water (blue) and human saliva (yellow) on EPET-nGO/P samples (ii).

Figure 5e lists the average water static contact angle, advancing contact angle, receding contact angle, hysteresis, and breakthrough pressure for EPET-nGO/P samples. The added PDMS coating slightly improves the fabric repellency properties. EPET-nGO/P samples are also superhydrophobic, with an average water static contact angle of 158 ± 1° (from 156 ± 1°) and water hysteresis of 6 ± 2° (from 9 ± 1°). The EPET-nGO/P samples transition from the Cassie−Baxter to Wenzel wetting state at an estimated contact line radius of 307 μm for a breakthrough pressure of 469 ± 75 Pa (from 282 ± 33 Pa). EPET-nGO/P samples have a higher breakthrough pressure than EPET-nGO samples due to the low surface energy layering of PDMS that covers any residual oxide groups of nGO-ODA.

Figure 5f shows the water static contact angle and hysteresis of EPET-nGO samples as a function of Taber rotary abrasion cycles. The average changes in static water contact angle and hysteresis of EPET-nGO/P are 2 ± 1° and 2 ± 1°, respectively, after 250 rotary abrasion cycles. Figure 5g shows the water static contact angle and hysteresis of EPET-nGO samples as a function of ultrasonic bleach washing cycles. The average changes in static water contact angle and hysteresis of EPET-nGO/P are 3 ± 1°and 2 ± 1°, respectively, after 33 bleach washing cycles. Video S1 shows water droplets rolling off EPET-nGO and EPET-nGO/P samples at a 10° tilt before and after rotary abrasion or bleach washing.

The PDMS layer is cross-linked which prevents color fastness, represented by the darker color seen in the optical image of Figure 5g and the small change in FTIR absorbance peaks after bleach washing in Figure S5. The presence of nGO-ODA can still be observed for EPET-nGO/P samples after 33 bleach washes at wavenumber 3129−3457 cm^{-1} by using FTIR (Figure S5). We conclude the additional PDMS treatment reduces the loss of nGO-ODA during bleach washing by acting as a low surface energy protective layer that offers chemical resistance to bleach. The wetting properties of EPET-nGO/P samples can withstand multiple bleach ultrasonic washing cycles.

Figure 6a compares the antiviral properties of pristine control PET, EPET-nGO, and EPET-nGO/P samples with HAdV5 (i), HSV-1 (ii), and CoV (iii). For EPET-nGO/P samples, antiviral properties consist of reducing titers of HAdV5 by 1.8 ± 1.0 log (98.6%), HSV-1 by 2.2 log ± 0.8 (99.4%), and CoV by 2.4 ± 0.2 log (99.6%) compared to controls. EPET-nGO/P samples may perform better than EPET-nGO samples across all virus stocks due to the improved repellency properties from the additional PDMS thin film. Figure 6b compares the amount of virus on fabric samples for HAdV5 (i), HSV-1 (ii), and CoV (iii) after 250 mechanical rotary abrasion cycles. EPET-nGO/P samples reduce titers of HAdV5 by 1.7 ± 1.0 log (98.1%), HSV-1 by 1.7 ± 1.0 log (98.0%), and CoV by 2.4 ± 0.2 log (99.6%) after 250 rotary abrasion cycles. Figure 6c compares the amount of virus on PET samples for HAdV5 (i), HSV-1 (ii), and CoV (iii) after 33 ultrasonic bleach washing cycles. EPET-nGO/P samples reduce titers of HAdV5 by 1.4 ± 0.2 log (95.7%), HSV-1 by 1.6 ± 0.4 log (97.3%), and CoV by 1.6 ± 0.4 log (97.6%) after 33 bleach washing cycles.

The antiviral property comes from a combination of antivirofouling and virus inactivation. The reduction of virus from the antivirofouling effect comes from the stable Cassie−Baxter wetting state. In a stable Cassie−Baxter wetting state, the area of fabric contact for virus particles in liquid to contaminate the fabric surface is significantly less due to the trapped pockets of air.[11] The combination of nanoroughness from the 2-dimensional graphene lattices and low surface energy from the ODA functional groups promote self-cleaning of extremely small (<600 nm) contaminants, such as viruses by reducing the area of contact.[29] The treated surface prevents liquid penetration and significantly reduces virus-to-surface contact area; therefore, fewer virus particles may attach to the surface.

Additionally, the 2d carbon nanomaterial nGO-ODA offers a virus inactivation effect. We perform virus inhibition experiments with 0.02% nGO-ODA and nGO-ODA with 0.01% PDMS (nGO-ODA/P) in fetal bovine serum (FBS) (Figure S6). The nGO-ODA alone demonstrates a reduction of HAdV5 by 0.88 ± 0.64 log (86.9%), while the nGO-ODA/P demonstrates a reduction of 0.24 ± 0.20 log (42.3%) in PFU per mL. The virus inactivation decreases with the presence of the PDMS.

The nGO-ODA treated fabric is antiviral through a combination of antivirofouling and virus inactivation with 1−2 log reduction of infectious virus quantities compared to controls. Virus inactivation may be beneficial when small aerosolized droplets contact the fabric. EPET-nGO/P samples repel more virus than EPET-nGO samples due to the higher

https://doi.org/10.1021/acsanm.1c03448
ACS Appl. Nano Mater. XXXX, XXX, XXX−XXX

robustness of the Cassie−Baxter wetting state. All in all, nGO-ODA treated fabric samples show a reduction in the amount of active virus present on the fabric for all types of virus tested, even after harsh durability tests proving its potential for reusable, functional PPE applications.

CONCLUSION

Virus infections cause a significant economical and social burden. There is a need for reusable, functional PPE to improve public health safety. This work demonstrates how coal-based carbon nanomaterials can be used to repel liquid and viruses in liquid on polyester fabric with long-lasting functionality. The fabric treatment fully repels water and human saliva droplets, even after mechanical abrasion or bleach washing. Most importantly, the fabric treatment shows reductions in virus quantities by 1−2 logs compared to controls for a range of enveloped and nonenveloped viruses, before and after mechanical abrasion or bleach washing cycles. The treatment is fluorine-free and utilizes cheap coal stocks for the potential of large scale production. We show a scalable, durable, superhydrophobic and antiviral functionality on common fabric for reusable PPE applications.

EXPERIMENTAL SECTION

Preparation of Octadecylamine-Functionalized Nano-Graphene Oxide. *Materials.* Coal char samples were produced by using a mild gasification process from Blue Gem coal provided by Carbon Technology Company in Bristol, VA.

Nano-Graphene Oxide Synthesis. Coal char was thermally treated at 1400 °C for 2 h under a nitrogen atmosphere for further carbonization. The obtained coal char was ground by using a shatterbox (SplexSamplePrep Shatterbox 8530) for 3 min. The ground coal char was then oxidized by using a mixture of concentrated sulfuric acid (95 wt %) and nitric acid (63 wt %). Typically, 5.0 g of ground coal char was added into a 1 L flask containing 150 mL of sulfuric acid and 50 mL of nitric acid under mixing, and then the temperature was raised to 100 °C and kept at this temperature for 24 h. Afterward, the mixture was naturally cooled to room temperature and was diluted with 2 L of DI water. The obtained solution was then neutralized with 10 wt % NaOH solution until pH = 3. Afterward, the solution was dialyzed by using a cross-flow dialysis filtration system (Repligen KrosFlo Research 2i TFF System) using a dialysis membrane with a molecular weight cutoff of 1.0 kDa for two times. The solution was subsequently acidified with 50 mL of 1 M H_2SO_4 solution and then dialyzed four more times to obtain the nano-graphene oxide.

Functionalization of Nano-Graphene Oxide with Octadecylamine. 200 mg of octadecylamine (ODA) was first dissolved in 20 mL of ethanol, and then octadecylamine solution was added into 100 mL of 1.0 mg/mL nano-graphene oxide (nGO) under mixing. The mixture was heated to 80 °C and kept at this temperature for 2 h. After natural cooling to room temperature, the mixture was vacuum filtrated to collect filter cake. Subsequently, the filter cake was baked at 130 °C for 2 h in an oven. The obtained product octadecylamine-functionalized nano-graphene oxide was finally dissolved in a mixture of hexane and ethanol (ratio of 95:5 v/v) at a concentration of 4 mg/mL. A 2:1 ratio of ODA:nGO was observed to be the ideal ratio for a coating solution. At lower ratios, the solution aggregates in organic solvents, and the graphene flakes are not fully functionalized. At larger ratios, the solution is mostly amines and too viscous for coating. The 2:1 ratio was chosen based on observational experiments in the lab.

Sample Preparation. *Materials.* PET knit wipes were purchased from Anticon. Acetone (99.5%), methanol (99.9%), and isopropyl alcohol (99.5%) were bought from VWR. PBS, FBS, KOH/water (45%), potassium permanganate, and PDMS (Sylgard) and were bought from Sigma-Aldrich. Coal-derived octadecylamine-functionalized nano-graphene oxide (nGO-ODA, 4 mg/mL in hexane) was provided by the National Energy Technology Laboratory (NETL). Extran MN 01 powdered detergent was purchased from MilliporeSigma. Household bleach was purchased from Giant Eagle. Food coloring was purchased from Amazon. Deionized water was used from a Millipore Academic A10 system with total organic carbon below 40 ppb. Human adenovirus type 5 (HadV5) and herpes simplex virus (HSV-1, Mckrae) were obtained from clinical isolates and frozen at −70 °C. Betacoronavirus were obtained from the American Type Culture Collection (ATCC), Manassas, VA (VR-1558). Virus stocks in PBS were prepared with A549 human lung carcinoma cells. The virus stocks were diluted in sterile PBS to the experimental titers used. Raw human saliva was collected in a test tube by one individual volunteer. Water and saliva were dyed blue and yellow, respectively, by adding 500 μL of food coloring to 10 mL of liquid in test tubes.

Sample Fabrication. The 0.5 in. by 0.5 in. square samples were cut from PET fabric. All samples were rinsed with acetone, methanol, and isopropyl alcohol and dried with nitrogen to eliminate possible contaminants. PET fabric was etched in 100 mL of 45% KOH:water for 30 min at 80 °C followed by 2 g of KMn_40_5 in 100 mL of water for 30 min at 80 °C to prepare etched PET (EPET). Then, samples were exhaustively dip-coated in nGO-ODA (4 mg/mL in hexane) and cured in an oven at 150 °C for 1 h to prepare etched PET-nGO-ODA (EPET-nGO). Lastly, etched PET nGO-ODA/PDMS (EPET-nGO/P) samples were prepared by soaking EPET-nGO in 500 μL of PDMS (Sylgard) at a 1:10 curing agent ratio diluted in 500 μL of hexane and curing in an oven at 150 °C for 2 h. Hexane was chosen as a solvent due to its low surface tension to easily wet the entire fabric surface during dip-coating.

Sample Characterization. The physical morphologies of samples were characterized by transmission electron microscopy (TEM, JEOL JEM2100F) and scanning electron microscopy (SEM, Zeiss Sigma 500 VP) at 5 kV. For SEM imaging, all samples were sputter-coated with 10 nm gold/palladium (80:20) by using a sputter-coater (Denton). The chemical compositions of samples were characterized by Fourier transform infrared spectroscopy (FTIR, Bruker Vertex-70LS) between 500 and 3600 cm^{-1} wavelengths. Raman spectra were obtained by using a Horiba (LabRam HR-Evolution) spectrometer with a 532 nm laser excitation source. The LabRam HR-Evolution software was used to subtract a baseline from the spectra. X-ray photoelectron spectroscopy (XPS) experiments were conducted with a PHI 5600ci spectrometer equipped with a hemispherical electron analyzer and a monochromatic Al Kα (1486.6 eV) radiation source. The pass energy of the analyzer was 55 eV. The powder samples were mounted on double-sided tape for analysis. All binding energies were calibrated to the C 1s peak located at 284.6 eV. MultiPak software was used for data processing, including determination of atomic concentrations.

Static, advancing, and receding contact angle measurements were taken in ambient air at approximately 25 °C and 30% relative humidity by using an optical tensiometer (Attension, 811 Theta). The 5 μL droplets at 25 °C for all test liquids were used for all wetting measurements. The hysteresis was tabulated for each treatment after measuring the advancing and receding contact angles during syringe-controlled water dispersion and withdrawal, respectively. Breakthrough pressure was measured by observing the contact angle and volume while a water droplet evaporates. When the droplet transitioned from the Cassie−Baxter to Wenzel state, the diameter of the droplet was tabulated to calculate the breakthrough pressure.

Durability Testing. Mechanical abrasion tests were performed by using a Taber Linear or Rotary Abrader (Model 5750) under the Ford Laboratory Test Method and ASTM standards for resistance to abrasion of textile treatments (BN 108-02 and D3884). Samples were fixed on a stage and subject to abrasion cycles by ceramic wheels (CS-10) under a load of 500 g in ambient air at approximately 25 °C and 30% relative humidity.

Washing cycles were performed by using a Powersonic P230 ultrasonic cleaner (Crest) under ASTM G131-96 standards for washing materials by ultrasonic techniques. A concentration of 10% bleach washing solution was chosen based on discussions with healthcare cleaning provider Cintas. A 10% bleach washing solution

https://doi.org/10.1021/acsanm.1c03448
ACS Appl. Nano Mater. XXXX, XXX, XXX−XXX

was prepared in a 10 mL test tube to create an efficient washing solution. Samples were submerged in bleach solution in Eppendorf tubes and ultrasonicated for 30 min at 80 W and 54 °C to complete one wash cycle. Afterward, samples were dried in ambient temperature before testing.

Virus Assays. Virus inhibition assays were performed by mixing nGO-ODA and nGO-ODA/P (nGO-ODA with PDMS, 0.1 mg/mL) with adenovirus or herpes virus in fetal bovine serum (FBS) at final concentration of 0.2 mg/mL. Solutions were vortexed and incubated for 1 h at room temperature. FBS was used because nGO-ODA does not dilute in PBS. After 1 h of incubation, 500 μL of ice-cold tissue culture media containing 20% FBS was added, then vortexed, and centrifuged for 1 min in the Eppendorf centrifuge to pellet any nGO-ODA or nGO-ODA/P. The supernatants were removed and plated with 0.1 mL of serial 10-fold dilutions in duplicate onto A549 monolayers in 24-well multiplates. The virus was absorbed for 1−3 h after which the wells were filled with 1 mL of tissue culture media containing 0.5% methyl cellulose. Plates were incubated for 5−6 days in 5% CO_2 and then fixed and stained with 0.5% gentian violet solution containing formalin, and the plaques were quantified.

Virus repelling assays were performed by completely submerging textile samples in 0.4 mL of virus/PBS in Eppendorf tubes with moderate shaking for 60 min (Stoval Belly Dancer, level 5) at room temperature. After shaking, samples were gingerly dipped twice in sterile PBS and submerged in Eppendorf tubes with 0.4 mL of PBS for PFU and 1.4 mL of PBS for $TCID_{50}$. Then, virions attached on the surface were removed from the samples into PBS by sonication at power 3 for 10 s (Qsonica, Model Q55) within the tubes. The liquid leftover was used to plate with cells and quantify plaques.

Virus titers (PFU per mL) for adenovirus and herpes simplex virus were determined by using standard plaque assay with A549 human lung carcinoma cells prepared in 24-well tissue culture plates. After 6−7 days incubation at 37 °C in 5% CO_2, the cells were fixed and stained with 0.5% gentian violet solution prepared in formalin, the number of plaques per well were counted under a dissecting microscope, and viral plaque forming unit titers were calculated.

Betacoronavirus (CoV) OC43 titers were determined by using the tissue culture infectious dose 50 ($TCID_{50}$) method with A549 human lung carcinoma cells prepared in 96-well tissue culture plates. After 14−16 days of incubation at 37 °C in 5% CO_2, the cells were fixed and stained with 0.5% gentian violet solution, wells were examined at 100× by using the inverted microscope, and a plus or negative sign was added depending on the cytopathic effect. Then, a $TCID_{50}$ calculator was used to determine the titer of stock in $TCID_{50}$ per milliliter. After the assays, Mann−Whitney U-tests were performed by using Matlab software for all comparisons between control and EPET-nGO-treated samples and between control and EPET-nGO/P-treated samples.

■ ASSOCIATED CONTENT

Supporting Information

The Supporting Information is available free of charge at https://pubs.acs.org/doi/10.1021/acsanm.1c03448.

Additional SEM images of coal-based functionalized nano-graphene oxide, detailed schematic of sample fabrication process, goniometer images of evaporating water droplets on samples from breakthrough pressure experiments, SEM images of samples after rotary abrasion or after ultrasonic bleach washing, FTIR spectra of samples after 33 bleach washes and virus inhibition results of nGO-ODA with HAdV5 and HSV-1 virus stocks (PDF)

Video S1 showing rolling water droplets at 10° tilt for EPET-nGO and EPET-nGO/P samples, before and after rotary abrasion or bleach washing (MP4)

■ AUTHOR INFORMATION

Corresponding Author

Paul W. Leu − *Department of Industrial Engineering, Department of Mechanical Engineering and Materials Science, and Department of Chemical Engineering, University of Pittsburgh, Pittsburgh, Pennsylvania 15261, United States*; Email: pleu@pitt.edu

Authors

Anthony J. Galante − *Department of Industrial Engineering, University of Pittsburgh, Pittsburgh, Pennsylvania 15261, United States*; orcid.org/0000-0002-1227-6771

Kathleen A. Yates − *Department of Ophthalmology, Charles T. Campbell Laboratory for Ophthalmic Microbiology, University of Pittsburgh School of Medicine, Pittsburgh, Pennsylvania 15213, United States*

Eric G. Romanowski − *Department of Ophthalmology, Charles T. Campbell Laboratory for Ophthalmic Microbiology, University of Pittsburgh School of Medicine, Pittsburgh, Pennsylvania 15213, United States*

Robert M. Q. Shanks − *Department of Ophthalmology, Charles T. Campbell Laboratory for Ophthalmic Microbiology, University of Pittsburgh School of Medicine, Pittsburgh, Pennsylvania 15213, United States*

Complete contact information is available at: https://pubs.acs.org/10.1021/acsanm.1c03448

Notes

The authors declare no competing financial interest.

■ ACKNOWLEDGMENTS

P.W.L. and A.J.G. acknowledge support from the U.S. National Science Foundation (NSF ECCS #1552 712). The authors thank Dr. Richard A. Wolfe from Carbon Technology Co. (Bristol, VA) for providing the coal char. The nano-graphene oxide synthesis, functionalization, and characterization were performed by Dr. Viet Hung Pham, Dr. Jennifer Weidman, Dr. Congjun Wang, and Dr. Christopher Matranga at the National Energy Technology Laboratory. The authors thank Dr. Viet Hung Pham, Dr. Jennifer Weidman, Dr. Congjun Wang, and Dr. Christopher Matranga for their help and expertise. The authors thank Dr. Daniel Lamont and Dr. Tan Susheng for additional help with sample characterization.

■ REFERENCES

(1) Barker, J.; Stevens, D.; Bloomfield, S. F. Spread and Prevention of Some Common Viral Infections in Community Facilities and Domestic Homes. *J. Appl. Microbiol.* **2001**, *91*, 7−21.

(2) (a) Lozano, R.; Naghavi, M.; Foreman, K.; Lim, S.; Shibuya, K.; Aboyans, V.; Abraham, J.; Adair, T.; Aggarwal, R.; Ahn, S. Y.; AlMazroa, M. A.; Alvarado, M.; Anderson, H. R.; Anderson, L. M.; Andrews, K. G.; Atkinson, C.; Baddour, L. M.; Barker-Collo, S.; Bartels, D. H.; Bell, M. L.; Benjamin, E. J.; Bennett, D.; Bhalla, K.; Bikbov, B.; Abdulhak, A. B.; Birbeck, G.; Blyth, F.; Bolliger, I.; Boufous, S.; Bucello, C.; Burch, M.; Burney, P.; Carapetis, J.; Chen, H.; Chou, D.; Chugh, S. S.; Coffeng, L. E.; Colan, S. D.; Colquhoun, S.; Colson, K. E.; Condon, J.; Connor, M. D.; Cooper, L. T.; Corriere, M.; Cortinovis, M.; Vaccaro, K. C. d.; Couser, W.; Cowie, B. C.; Criqui, M. H.; Cross, M.; Dabhadkar, K. C.; Dahodwala, N.; Leo, D. D.; Degenhardt, L.; Delossantos, A.; Denenberg, J.; Jarlais, D. C. D.; Dharmaratne, S. D.; Dorsey, E. R.; Driscoll, T.; Duber, H.; Ebel, B.; Erwin, P. J.; Espindola, P.; Ezzati, M.; Feigin, V.; Flaxman, A. D.; Forouzanfar, M. H.; Fowkes, F. G. R.; Franklin, R.; Fransen, M.; Freeman, M. K.; Gabriel, S. E.; Gakidou, E.; Gaspari, F.; Gillum, R. F.;

Gonzalez-Medina, D.; Halasa, Y. A.; Haring, D.; Harrison, J. E.; Havmoeller, R.; Hay, R. J.; Hoen, B.; Hotez, P. J.; Hoy, D.; Jacobsen, K. H.; James, S. L.; Jasrasaria, R.; Jayaraman, S.; Johns, N.; Karthikeyan, G.; Kassebaum, N.; Keren, A.; Khoo, J.-P.; Knowlton, L. M.; Kobusingye, O.; Koranteng, A.; Krishnamurthi, R.; Lipnick, M.; Lipshultz, S. E.; Ohno, S. L.; Mabweijano, J.; MacIntyre, M. F.; Mallinger, L.; March, L.; Marks, G. B.; Marks, R.; Matsumori, A.; Matzopoulos, R.; Mayosi, B. M.; McAnulty, J. H.; McDermott, M. M.; McGrath, J.; Memish, Z. A.; Mensah, G. A.; Merriman, T. R.; Michaud, C.; Miller, M.; Miller, T. R.; Mock, C.; Mocumbi, A. O.; Mokdad, A. A.; Moran, A.; Mulholland, K.; Nair, M. N.; Naldi, L.; Narayan, K. M. V.; Nasseri, K.; Norman, P.; O'Donnell, M.; Omer, S. B.; Ortblad, K.; Osborne, R.; Ozgediz, D.; Pahari, B.; Pandian, J. D.; Rivero, A. P.; Padilla, R. P.; Perez-Ruiz, F.; Perico, N.; Phillips, D.; Pierce, K.; Pope, C. A.; Porrini, E.; Pourmalek, F.; Raju, M.; Ranganathan, D.; Rehm, J. T.; Rein, D. B.; Remuzzi, G.; Rivara, F. P.; Roberts, T.; León, F. R. D.; Rosenfeld, L. C.; Rushton, L.; Sacco, R. L.; Salomon, J. A.; Sampson, U.; Sanman, E.; Schwebel, D. C.; Segui-Gomez, M.; Shepard, D. S.; Singh, D.; Singleton, J.; Sliwa, K.; Smith, E.; Steer, A.; Taylor, J. A.; Thomas, B.; Tleyjeh, I. M.; Towbin, J. A.; Truelsen, T.; Undurraga, E. A.; Venketasubramanian, N.; Vijayakumar, L.; Vos, T.; Wagner, G. R.; Wang, M.; Wang, W.; Watt, K.; Weinstock, M. A.; Weintraub, R.; Wilkinson, J. D.; Woolf, A. D.; Wulf, S.; Yeh, P.-H.; Yip, P.; Zabetian, A.; Zheng, Z.-J.; Lopez, A. D.; Murray, C. J. Global and regional mortality from 235 causes of death for 20 age groups in 1990 and 2010: a systematic analysis for the Global Burden of Disease Study 2010. *Lancet* **2012**, *380*, 2095−2128.

(3) Morens, D. M.; Fauci, A. S. Emerging infectious diseases: threats to human health and global stability. *PLoS Pathog.* **2013**, *9*, No. e1003467.

(4) Kraay, A. N.; Hayashi, M. A.; Hernandez-Ceron, N.; Spicknall, I. H.; Eisenberg, M. C.; Meza, R.; Eisenberg, J. N. Fomite-mediated transmission as a sufficient pathway: a comparative analysis across three viral pathogens. *BMC Infect. Dis.* **2018**, *18*, 540.

(5) Nii-Trebi, N. I. Emerging and Neglected Infectious Diseases: Insights, Advances, and Challenges. *BioMed. Research International* **2017**, *2017*, No. e5245021.

(6) Antonelli, G.; Turriziani, O. Antiviral therapy: old and current issues. *Int. J. Antimicrob. Agents* **2012**, *40*, 95−102.

(7) Karim, N.; Afroj, S.; Lloyd, K.; Oaten, L. C.; Andreeva, D. V.; Carr, C.; Farmery, A. D.; Kim, I.-D.; Novoselov, K. S. Sustainable Personal Protective Clothing for Healthcare Applications: A Review. *ACS Nano* **2020**, *14*, 12313−12340.

(8) Kilinc, F. S. A Review of Isolation Gowns in Healthcare: Fabric and Gown Properties. *J. Eng. Fibers Fabr.* **2015**, *10*, 155892501501000313.

(9) Overcash, M. A. Comparison of Reusable and Disposable Perioperative Textiles: Sustainability State-Of-The-Art 2012. *Anesth. Analg.* **2012**, *114*, 1055−1066.

(10) Querido, M. M.; Aguiar, L.; Neves, P.; Pereira, C. C.; Teixeira, J. P. Self-disinfecting surfaces and infection control. *Colloids Surf., B* **2019**, *178*, 8−21.

(11) Galante, A. J.; Haghanifar, S.; Romanowski, E. G.; Shanks, R. M. Q.; Leu, P. W. Superhemophobic and Antivirofouling Coating for Mechanically Durable and Wash-Stable Medical Textiles. *ACS Appl. Mater. Interfaces* **2020**, *12*, 22120−22128.

(12) Liu, S.; Zeng, T. H.; Hofmann, M.; Burcombe, E.; Wei, J.; Jiang, R.; Kong, J.; Chen, Y. Antibacterial Activity of Graphite, Graphite Oxide, Graphene Oxide, and Reduced Graphene Oxide: Membrane and Oxidative Stress. *ACS Nano* **2011**, *5*, 6971−6980.

(13) Serrano-Aroca, Á.; Takayama, K.; Tuñón-Molina, A.; Seyran, M.; Hassan, S. S.; Pal Choudhury, P.; Uversky, V. N.; Lundstrom, K.; Adadi, P.; Palù, G.; Aljabali, A. A. A.; Chauhan, G.; Kandimalla, R.; Tambuwala, M. M.; Lal, A.; Abd El-Aziz, T. M.; Sherchan, S.; Barh, D.; Redwan, E. M.; Bazan, N. G.; Mishra, Y. K.; Uhal, B. D.; Brufsky, A. Carbon-Based Nanomaterials: Promising Antiviral Agents to Combat COVID-19 in the Microbial-Resistant Era. *ACS Nano* **2021**, *15*, 8069−8086.

(14) Donskyi, I. S.; Nie, C.; Ludwig, K.; Trimpert, J.; Ahmed, R.; Quaas, E.; Achazi, K.; Radnik, J.; Adeli, M.; Haag, R.; Osterrieder, K. Graphene Sheets with Defined Dual Functionalities for the Strong SARS-CoV-2 Interactions. *Small* **2021**, *17*, 2007091.

(15) Łoczechin, A.; Séron, K.; Barras, A.; Giovanelli, E.; Belouzard, S.; Chen, Y.-T.; Metzler-Nolte, N.; Boukherroub, R.; Dubuisson, J.; Szunerits, S. Functional Carbon Quantum Dots as Medical Countermeasures to Human Coronavirus. *ACS Appl. Mater. Interfaces* **2019**, *11*, 42964−42974.

(16) Zhong, H.; Zhu, Z.; Lin, J.; Cheung, C. F.; Lu, V. L.; Yan, F.; Chan, C.-Y.; Li, G. Reusable and Recyclable Graphene Masks with Outstanding Superhydrophobic and Photothermal Performances. *ACS Nano* **2020**, *14*, 6213−6221.

(17) Huang, P.-S.; Qin, F.; Lee, J.-K. Role of the Interface between Ag and ZnO in the Electric Conductivity of Ag Nanoparticle-Embedded ZnO. *ACS Appl. Mater. Interfaces* **2020**, *12*, 4715−4721.

(18) Achagri, G.; Essamlali, Y.; Amadine, O.; Majdoub, M.; Chakir, A.; Zahouily, M. Surface modification of highly hydrophobic polyester fabric coated with octadecylamine-functionalized graphene nanosheets. *RSC Adv.* **2020**, *10*, 24941−24950.

(19) Yan, H.; Zhou, H.; Ye, Q.; Wang, X.; Cho, C. M.; Tan, A. Y. X.; Xu, J. Engineering polydimethylsiloxane with two-dimensional graphene oxide for an extremely durable superhydrophobic fabric coating. *RSC Adv.* **2016**, *6*, 66834−66840.

(20) *Graphite prices globally by flake grade 2011−2020*. https://www.statista.com/statistics/452\\,304/graphite-prices-worldwide-prediction-by-flake-grade/.

(21) *Thermal coal price 2013−2020*. https://www.statista.com/statistics/214\\,236/thermal-coal-prices-since-2003/.

(22) Discussions with Cintas.

(23) Rutala, W. A.; Weber, D. J. Uses of inorganic hypochlorite (bleach) in health-care facilities. *Clin. Microbiol. Rev.* **1997**, *10*, 597−610.

(24) Zhong, H.; Zhu, Z.; You, P.; Lin, J.; Cheung, C. F.; Lu, V. L.; Yan, F.; Chan, C.-Y.; Li, G. Plasmonic and Superhydrophobic Self-Decontaminating N95 Respirators. *ACS Nano* **2020**, *14*, 8846−8854.

(25) Wadell, G. Molecular Epidemiology of Human Adenoviruses. *Molecular Biology of Adenoviruses* **1984**, *110*, 191−220.

(26) Wald, A.; Corey, L. In *Human Herpesviruses: Biology, Therapy, and Immunoprophylaxis*; Arvin, A., Campadelli-Fiume, G., Mocarski, E., Moore, P. S., Roizman, B., Whitley, R., Yamanishi, K., Eds.; Cambridge University Press: Cambridge, 2007.

(27) Lavi, E.; Weiss, S. R. In *Clinical and Molecular Aspects of Neurotropic Virus Infection*; Gilden, D. H., Lipton, H. L., Eds.; Developments in Medical Virology; Springer: Boston, MA, 1989; pp 101−139.

(28) Rigby, A. J.; Anand, S. C.; Horrocks, A. R. Textile Materials for Medical and Healthcare Applications. *J. Text. Inst.* **1997**, *88*, 83−93.

(29) Geyer, F.; D'Acunzi, M.; Sharifi-Aghili, A.; Saal, A.; Gao, N.; Kaltbeitzel, A.; Sloot, T.-F.; Berger, R.; Butt, H.-J.; Vollmer, D. When and how self-cleaning of superhydrophobic surfaces works. *Science Advances* **2020**, *6*, No. eaaw9727.

(30) Nosonovsky, M.; Bhushan, B. Biomimetic Superhydrophobic Surfaces: Multiscale Approach. *Nano Lett.* **2007**, *7*, 2633−2637.

(31) Xiu, Y.; Liu, Y.; Hess, D. W.; Wong, C. P. Mechanically Robust Superhydrophobicity on Hierarchically Structured Si Surfaces. *Nanotechnology* **2010**, *21*, 155705.

https://doi.org/10.1021/acsanm.1c03448
ACS Appl. Nano Mater. XXXX, XXX, XXX−XXX